Scanning Microscopy Vol. 12, No. 2, 1998 (Pages 285-299) 0891-7035/98$5.00+.25
Scanning Microscopy International, Chicago (AMF O'Hare), IL 60666 USA

CATHODOLUMINESCENCE IN THE SCANNING ELECTRON MICROSCOPE: APPLICATION TO LOW-DIMENSIONAL SEMICONDUCTOR STRUCTURES

Anders Gustafsson* and Eli Kapon

Institut de Micro et Optoélectronique, Departement de Physique,
Ecole Polytechnique Fédérale Lausanne, CH-1015 Lausanne, Switzerland

(Received for publication August 1, 1996 and in revised form December 2, 1996)

Abstract

Cathodoluminescence is a very powerful tool for the characterization of low-dimensional semiconductor structures. The high spatial resolution is especially useful when studying low-dimensional structures like quantum wires and quantum dots. In combination with the normal secondary electron detection mode it is possible to locate specific areas of the sample. This can for instance be an area of a quantum-well substrate that has been patterned by etching, to form quantum wires. In more complicated quantum-wire structures, with several luminescence peaks, monochromatic imaging and spot mode spectra can be used to identify the spatial origin of these peaks. The large range of available probe currents is useful for studying the excitation-density dependence of the emission peaks. The emission from excited subbands of quantum wires can be observed at higher excitation densities. In the ultimate limit, the emission from single impurities can be identified and their position located in these quantum wires.

Key Words: Cathodoluminescence, low-dimensional semiconductor structures, quantum well, quantum wire, vertical quantum well, non-planar growth, scanning electron microscope, transmission electron microscope.

*Address for correspondence:
Anders Gustafsson
Solid State Physics
Lund University
S-221 00 Lund, Sweden
Telephone number: +46-(0)46-222 0337
FAX number: +46-(0)46-222 3637
E-mail: anders.gustafsson@ftf.lth.se

Introduction

Cathodoluminescence (CL) in the scanning electron microscope (SEM) or the scanning transmission electron microscope (STEM) is a very useful tool for the characterization of low-dimensional semiconductor structures. To obtain spatial resolution, the SEM/STEM provides a highly focused electron beam that can be positioned at specific sites to obtain spot mode spectra. The beam can also be scanned over the sample to record images and to obtain spatially averaged spectra. The normal facilities of the SEM/STEM, e.g., topographical imaging and X-ray analysis, can be used to identify regions of interest as well as to avoid artifacts. Typical artifacts include dust particles or fragments of the substrate lying on the surface, scratches and cracks on the surface. The technique has inherently a potential for sub-micron resolution, depending on the experimental conditions and the sample (Christen *et al.,* 1991). Such resolution can be applied to large areas, limited primarily by the field of view of the light collection optics, which is typically 100×100 μm^2. Larger areas can be easily accessed by using the precision positioning system of the SEM/STEM, where the size of the sample is limited by the size of the sample holder. This varies from system to system: In the SEM, generally sample sizes of up to 50×50 mm^2 can be used, whereas in the STEM, the samples are often limited by the 3 mm diameter of the STEM sample holder. In the rest of this article, we will limit ourselves to SEM-based CL work.

The spatial resolution is mainly governed by three factors: the spot size of the focused electron beam, the spreading of the electrons of the beam inside the sample (leading to a finite *generation volume*), and diffusion of the generated secondary carriers within the sample (Yacobi and Holt, 1990). Other influences on the resolution are related to the sample itself in terms of sample geometry, internal absorption and reflection, and secondary photon emission (fluorescence or photon recycling). The spot size is determined by the SEM and is generally a function of probe current; a lower current, generally, results in a smaller spot size. The acceleration voltage also influences the spot size for a given probe current: a higher voltage generally leads to a smaller spot size. More important, however, is that the

penetration depth of the primary electrons increases with acceleration voltage. The larger penetration depth, in turn, gives a larger lateral spreading of the electrons in the sample resulting in a bigger generation volume. The diffusion length, on the other hand, is a material parameter, which can be influenced by the sample temperature. For a given excitation density and sample temperature the only free parameter is the acceleration voltage, which determines the size of the generation volume and therefore its increase might have a severe influence on the resolution. A rule of thumb is that the width of the generation volume roughly equals the penetration depth. The choice of the appropriate acceleration voltage is therefore essential for achieving the best resolution. Not taking into account the slight increase of the spot size of the SEM with reduced acceleration voltage, the best resolution is obtained with the lowest possible voltage that still gives a substantial direct excitation of the region of interest. If too high a voltage is used, the generation volume will be excessively wide, with reduced resolution as a consequence. On the other hand, if the voltage is too low, most of the excitation might take place in the sample volume above the region of interest. The emission of interest is then the result of carriers that have reached this region via diffusion, again with reduced spatial resolution as a consequence.

Figure 1 demonstrates the different modes of the CL technique, in a simple model. For the purpose of illustration, we are using a sample containing an array of quantum wires (QWRs). We also limit this demonstration to an ideal case, where both the generation volume and the diffusion length are smaller than the features in the sample. In a spatially averaged spectrum, recorded with the beam scanning over an area, two emission peaks appear: one from the QWR and one from the barrier material. This is what a non-spatially resolved technique would yield. If the scan is stopped, and the beam positioned on a QWR, the emission from the QWR would be recorded. If the beam is positioned between two QWRs, the emission from the barrier would be recorded. This mode is known as *spot mode*. If the photon energy of either of the emission peaks is chosen for *monochromatic imaging*, their spatial origin can be imaged. Schematic images in both top and side view of the respective emission peaks are shown in Figure 1. In these schematic images (as well as all real images discussed below) black illustrates low CL intensity and white corresponds to a high CL intensity.

In reality, it is rare that the structures studied by CL are significantly larger than the generation volume and the diffusion length. This modifies the illustrations in Figure 1. In the spot mode spectra it is often difficult to totally isolate one single emission peak. The monochromatic images will show a continuous grey scale rather than the black and white contrast. Generally, CL images show the contrast variations rather than the absolute intensities: black

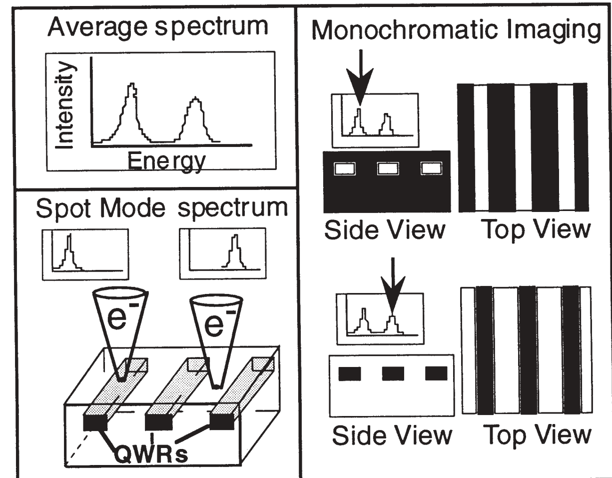

Figure 1. A QWR sample is used to illustrate the CL technique. A spatially averaged spectrum can be recorded with the beam scanning over an area containing several QWRs. The spectrum contains the peaks emanating from the QWR and the barrier. In spot mode, the spectra from the QWR and the barrier area can be isolated. In the imaging mode, a certain spectral feature can be imaged and the corresponding image reflects the spatial origin of the spectral feature.

corresponds to a finite and minimum intensity rather than the absolute zero intensity.

Most of the samples that are studied by CL are generally not designed only for this purpose. This means that their geometry is usually not optimized for a potentially high spatial resolution. These samples are often analyzed by CL in order to identify the spatial origin of the various spectral components. However, specially designed samples, with the layers to be characterized positioned near the surface (< 50 nm) for top view observation and cleaved surfaces for side view observation, can be prepared. These types of structures are typically observed with an acceleration voltage of 1 - 5 kV. Resolution in images down to 45 nm has been demonstrated (Grundmann *et al.,* 1994).

Quantum Wells

A quantum well (QW) is the simplest category of low-dimensional structures. Structurally, a QW is a thin sheet of low bandgap material embedded in a matrix of high bandgap material (Dingle, 1975). In the ideal case the thin sheet is completely uniform in thickness and the interfaces are infinitely sharp. From a quantum mechanical point of view, this leads to a particle in a one dimensional (1D) box behaviour for the electrons and holes in the direction

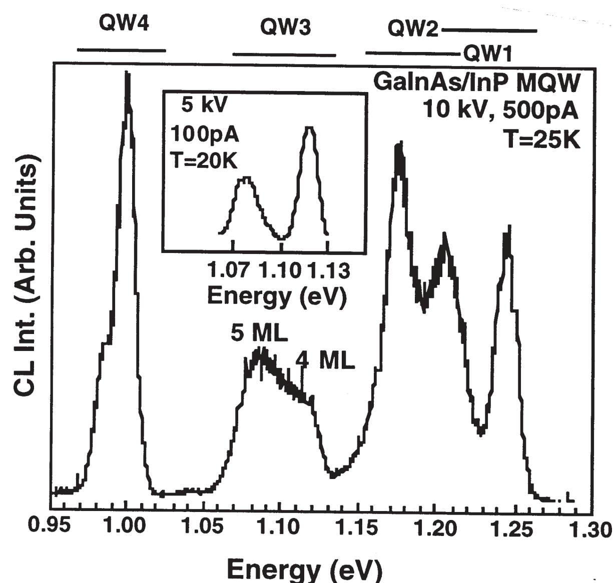

Figure 2. A typical spectrum from a sample containing a stack of 4 different GaInAs/InP QWs. The spectrum is recorded over 10x10 μm². Each group of peaks originates in a single QW, as indicated on the upper abscissa. The inset shows a part of the spectrum re-recorded with higher spectral resolution and lower excitation density.

perpendicular to the sheet. The effective bandgap of the QW is determined by the bandgap of the QW material, the difference in bandgap between the two materials and the thickness, or width, of the QW (Dingle, 1975). For thin QWs, a very small difference in the width of the QW results in a change of the effective bandgap in the order of per cent. In fact, a difference of 1 monolayer (1 ML, which is the thinnest complete layer of the semiconductor) can introduce large (several %) changes in the effective bandgaps. In the (100) direction 1 ML is half the lattice constant (a/2, e.g., in GaAs 1 ML is 0.283 nm).

In reality there are no perfect QWs. All real QW structures exhibit, to some extent, graded interfaces, thickness variations and composition variations. The quality of a QW is often related to the photon emission in terms of the full width at half maximum (FWHM) of the luminescence peak (Herman *et al.,* 1991). This, in turn, is related to the homogeneity of the QW that is investigated. In fact, the luminescence spectrum reflects variation in the QW potential (i.e., thickness and composition), averaged over the exciton Bohr diameter (~20 nm in GaAs). Flat areas, i.e. with interfaces defined within one ML, on the scale of the exciton result in sharp emission peaks, one peak for each thickness of the QW (Herman *et al.,* 1991; Warwick *et al.,* 1990). The emission from small areas (typically 10×10 μm²) of a highly uniform single QW, often exhibits two or three peaks in the emission. These peaks correspond to a series of thicknesses of the QW differing by single ML. Furthermore, over large areas (several mm), there can be a large scale thickness gradient or variation, due to inhomogeneities in the growth rate (Seifert *et al.,* 1990). If however, the flat areas of the QW are smaller than the exciton diameter, the emission energy will correspond to the effective thickness the exciton averages over when it recombines. This effective thickness can be a non-integer ML thickness and can vary from area to area. The spatially averaged spectra will therefore contain one broad peak, which is the envelope of all the effective thicknesses within the QW (Herman *et al.,* 1991).

Figure 2 shows a typical spectrum from a sample containing a stack of four GaInAs/InP QWs of different thicknesses. The spectrum is recorded over an area of 10×10 μm². In this sample, grown by low-pressure metalorganic chemical vapour deposition (MOCVD), there is an intentional thickness gradient over the 25 mm length of the sample. This can be observed by recording a series of spectra along the gradient. Each of the QWs shows one or two peaks and each peak originates in a specific thickness, where two adjacent peaks correspond to emission from areas that differ in thickness by 1 ML (Liu *et al.,* 1993). This can be confirmed by examining the consecutive spectra. Each single peak reappears in the same position in the consecutive spectra, but the intensity ratio of the peaks emanating from a single QW varies.

As discussed above, an analysis of the shape and width of the emission peaks of the QW can reveal if the ML-flat areas are smaller or larger than the exciton Bohr diameter (Herman *et al.,* 1991). In the latter case, the actual size of the ML-flat areas cannot be determined by lineshape analysis alone. Using the low-voltage range of CL imaging ML-flat areas larger than ~0.5 μm can be accessed. Imaging of extended ML-flat islands in QWs was first reported in the AlGaAs/GaAs system, where island sizes of ~1 μm (Petroff *et al.,* 1987) and 6-8 μm (Bimberg *et al.,* 1987) were reported. Not only the AlGaAs system, but also lattice matched GaInAs/InP exhibits the extended ML-flat areas (Herman *et al.,* 1991; Nilsson *et al.,* 1990). Following these first reports, the subject of extended ML-flat islands has attracted considerable attention, mainly regarding the influence of growth conditions. Figure 3 shows a typical pair of monochromatic top view images of a GaInAs QW sandwiched between InP barriers, recorded at 20 K, 5 kV and 100 pA. The emission from this area exhibits two well defined and separated peaks, attributed to excitonic recombination in areas of 4 and 5 ML thickness, respectively. (The notation 4 and 5 ML does not necessarily refer to the exact number of pure GaInAs ML in between InP barriers,

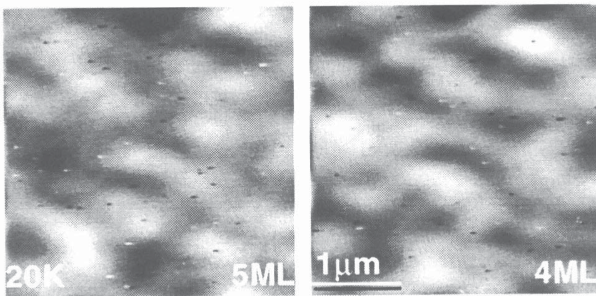

Figure 3. Top view images recorded at 20K with the detection energy set on either the 4 ML peak or the 5 ML peak of QW3 in Figure 2.

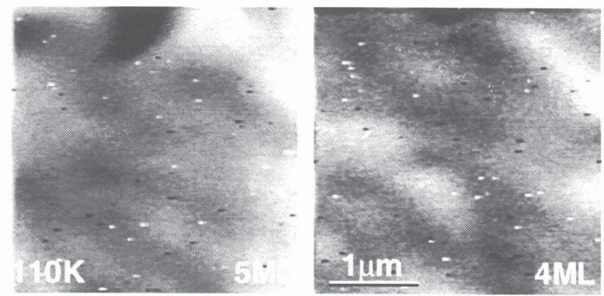

Figure 4. Top view images recorded over the same area as in Figure 3. The sample temperature was 100K and the detecetion energy set on either the 4ML peak or the 5ML peak of QW3.

but is an effective width. The thickness 1 ML is the thinnest QW produced by exchange processes at the interface during growth. 5 ML is therefore 4 ML pure GaInAs plus the interface layers.) The two images quite are complementary: Most bright areas in one image corresponds to dark areas in the second image, and vice versa. The lateral scale of the contrast variations in these images is 0.5-1 μm and the intensity varies from 100 down to 35 %.

It is tempting to interpret these images as direct maps of the areas of the two thicknesses that correspond to the peaks in the emission spectra. This seems plausible, especially since the collective effect of the probe size and the generation volume can be expected to be smaller than the features observed in the images. However, the images can be affected by diffusion of the excitons involved. This is often a severe problem of the CL technique when the features that are investigated are on the order of or smaller than the diffusion length: *The intensity of the emission is recorded as a function of the position of the electron beam, with no consideration of the carrier diffusion in the sample.* In a simple case, diffusion simply leads to a reduction of the contrast in the images. However, the situation is more complicated for diffusion in a QW, where the energy difference between areas of different thickness can impose restrictions on the direction of the diffusion. The energy required, for an exciton to go from a thicker area to a thinner area can be much larger than the thermal energy (kT) and, therefore, this path can be effectively blocked. The diffusion in the opposite direction can in principle flow unhindered (Gustafsson and Samuelson, 1994). The influence of diffusion can be demonstrated in a series of pairs of images of the 4 and 5 ML peaks, recorded at different temperatures. In this case the difference in quantization energy between the two thicknesses is about 35 meV. The images of Figure 3 are recorded at 20 K and the images of exactly the same area recorded at 110 K are shown in Figure 4. As the temperature increases, the excitons become more mobile and the diffusion length increases. This is reflected in the images, where the features get less distinct with increasing temperature. At 20 K, the features are ~ 0.5 - 1 μm, whereas at 110 K the features in exactly the same area are ~ 1 -2 μm. What is most important is that the 110 K images still show complementary behaviour, but with larger features and lower contrast. The lesson that can be learnt from this is that care must be taken in order to correctly interpret CL images. In the case above, what appear to be solid areas of 4 and 5 ML, is probably a variation in the density of smaller islands of 4 and 5 ML (Gustafsson and Samuelson, 1994).

The over-estimation of the size of the individual islands can be demonstrated in a different type of sample. This consists of a highly strained, thin layer of InAs sandwiched between InP barriers. Instead of relaxing by formation of misfit dislocations, the film relaxes by formation of three-dimensional islands, in a growth mode known as the Stranski-Krastanow mode (Grundmann *et al.,* 1995a; Leon *et al.,* 1995). For a growth time corresponding to ~2 full ML of InAs, the resulting average CL spectrum contains a series of peaks, which is shown in Figure 5. The peaks correspond to a series of thicknesses, again separated by 1 ML, ranging from 1 to 8 ML, covering the spectral range from the InP barrier to the cut-off of the Ge-pin diode used to detect the emission in this experiment. The spectrum was recorded at 25 K and 5 kV with a probe current of 100 pA, conditions similar to the lattice matched QW experiments discussed above. Figure 6 shows top view images of the 1 and 2 ML emission. A similar pattern of a series of bright and dark spots on a 0.5 μm scale can be observed in the images corresponding to the other peaks as well. This is the same scale as in the low temperature images of the lattice matched QWs discussed above. The only deviation from this is the InP barrier peak, which does

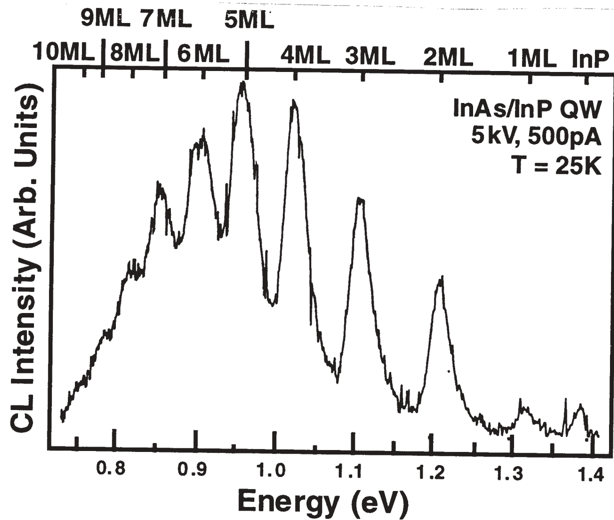

Figure 5. A typical average spectrum from an InAs/InP QW structure, containing small islands of several thicknesses. Each thickness is represented by one peak in a series from 1 to 8 ML.

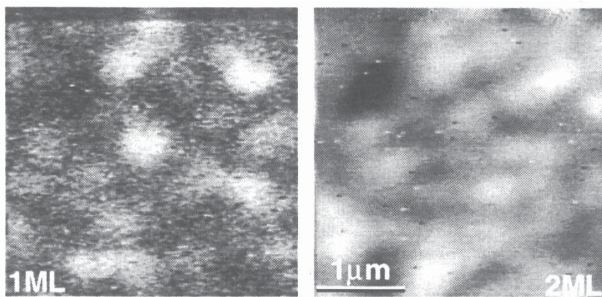

Figure 6. Monochromatic images of the 1 and 2 ML peaks of the sample in Figure 5. Though the extensions of the islands are expected to be 20-50 nm, the bright spots from single islands appear on a 0.5 μm scale.

not exhibit any intensity variations at all. Furthermore, there is no correlation (or anti-correlation) in the series of images of the InAs islands: a bright spot in one image does not exclude this area from being bright in any of the other images. In this case we are clearly observing individual and disconnected small objects with different thicknesses. From transmission electron microscope (TEM) studies (Araújo *et al.,* 1994; Carlin *et al.,* 1992) it was observed that the typical extension of these islands was 20-50 nm, with spacing of about 200 nm. This explains the apparent overlap in the images of the various thicknesses, as both the separation and the size are significantly smaller than the resolution.

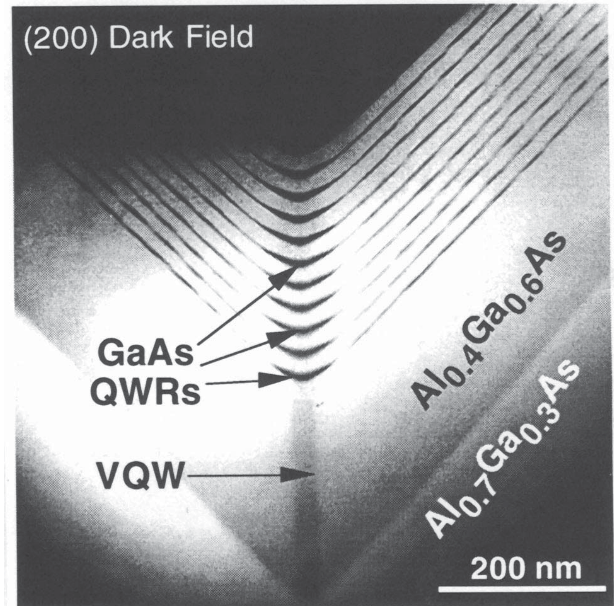

Figure 7. DF, cross-sectional TEM image of a typical stack of 10 identical QWRs grown on a V-grooved substrate. The GaAs QWRs have a crescent shape and appear black in the image, whereas the AlGaAs barriers appear grey. The structure is grown on a 3.5 μm period grating, very suitable for CL imaging.

Quantum Wires Grown on Non-Planar Substrates

One of the areas where the CL technique really comes to the fore is in the studies of quantum wires (QWRs). A QWR can be described as a stripe of low bandgap material in a matrix of high bandgap material (Forchel *et al.,* 1988; Kapon, 1992; Merz and Petroff 1991). As a result, the quantum confinement occurs in 2 dimensions, leaving one dimension for free movement, and thus a 1D system is realized. This is an area where the CL technique is very useful, not just for the very local nature of the excitation and the potentially high resolution, but also for the ability to work with “open eyes” in the normal SEM mode, with which the topography of the sample can be studied. In this mode it is normally possible to locate most of these types of structures, since most of the fabrication methods tend to leave traces of the structure on the surface of the sample. A typical example is a commonly used technique for QWR fabrication, where free-standing ridges are etched out in an existing QW substrate (Clausen *et al.,* 1990a; Forchel *et al.,* 1988). These ridges can be observed in the SEM mode. This technique for the fabrication of QWRs is simple and can be quite efficient, but suffers from several drawbacks. The

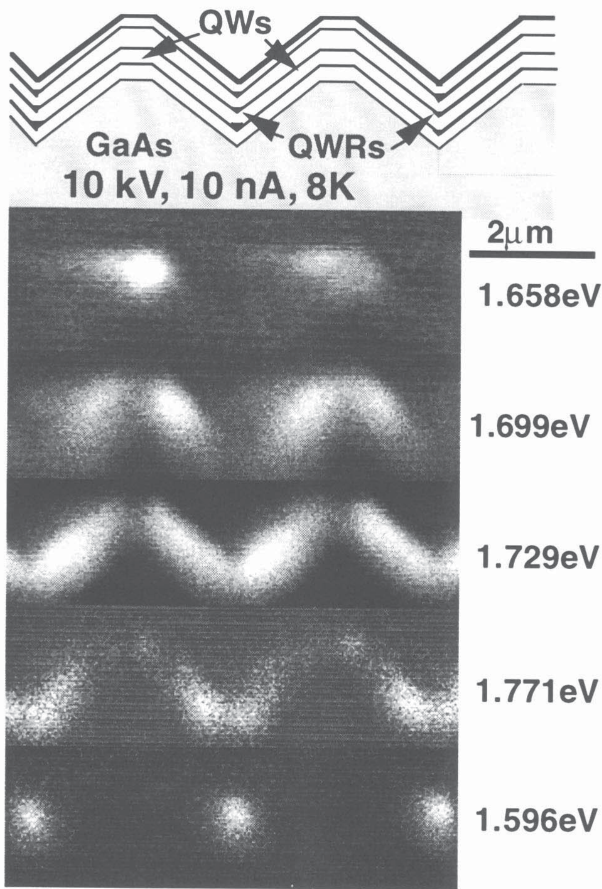

Figure 8. Two periods of the QWR structure of Figure 7 in side view. The QWR at the bottom of the groove emits at 1.60 eV, the top QW emits at 1.66 eV and the side QW emits at 1.73 eV. There is also a trend for the side wall to be thinner at the bottom of the groove (1.77 eV) than at the top (1.70 eV).

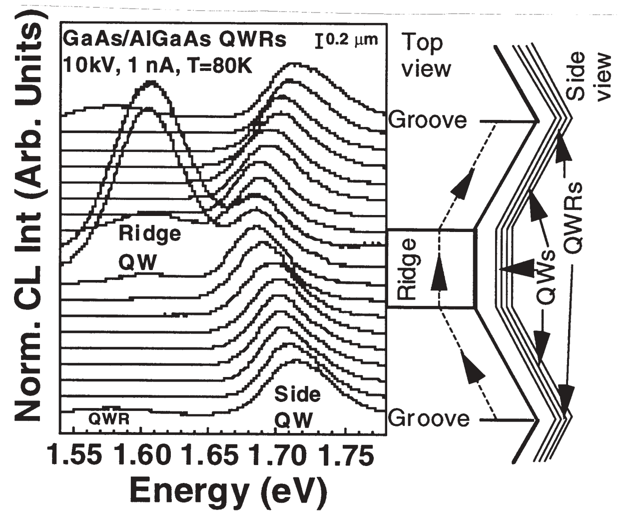

Figure 9. A series of top view, spot mode spectra, going from the bottom of one groove to the adjacent groove of a sample grown under the same conditions as the sample in Figure 8. The thickness gradient of the side QW is also apparent in this series, where the emission shifts from 1.72 eV at the bottom of the groove to 1.69 eV at the top of the groove. The dashed line in the schematic illustration on the right shows the path of the line scan.

variations of the width of the ridge can introduce severe fluctuations of the energy levels of the QWRs and the etched sides of the structure can act as non-radiative recombination centres.

One of the more attractive ways to fabricate QWRs is to grow the structures directly on non-planar substrates (Kapon *et al.,* 1987). This especially applies to the approach of self-ordering of the QWRs by MOCVD growth on V-grooved substrates (Kapon *et al.,* 1992a). One of the main driving forces in the fabrication of QWRs is the prospect for making lasers with advan- tageous properties. Most notably this is the extremely low threshold currents that are expected, which to some extent has been demonstrated (Tiwari, 1994; Tiwari *et al.,* 1994). A typical structure consisting of a stack of 10 QWRs is shown in the dark field (DF) TEM image of Figure 7, where the GaAs QWs/QWRs appear dark and the AlGaAs barriers are light grey. The cross section of the QWRs can be made on the order of 10×5 nm^2, resulting in a spacing of the 1D subbands of >25 meV, which is one of the criteria for the fabrication of room temperature devices based on QWRs (Kapon *et al.,* 1992a). The self-ordering approach for making these QWRs uses the difference in surface diffusion-length and sticking coefficient of the growth species on the different planes involved. What is more important is the resulting shape of the growth front at the bottom of the groove, characterized by the radius of curvature at the tip of the V (Kapon *et al.,* 1995a). This is especially interesting in the AlGaAs system, where this radius decreases with increasing Al content. This means that a thin, low Al content layer (practically this is pure GaAs) grown on a high Al content buffer exhibits an increase in the radius, i.e., resulting in a crescent shaped layer in the groove. If the low Al content layer is grown to a QW thickness, the finite width of the crescent leads to size quantization in the direction across the groove, in addition to the quantization in the growth direction. This two-dimensional quantization is the signature of a QWR. The value of the radius of curvature determines the minimum achievable width of the QWR. A second high Al content layer grown

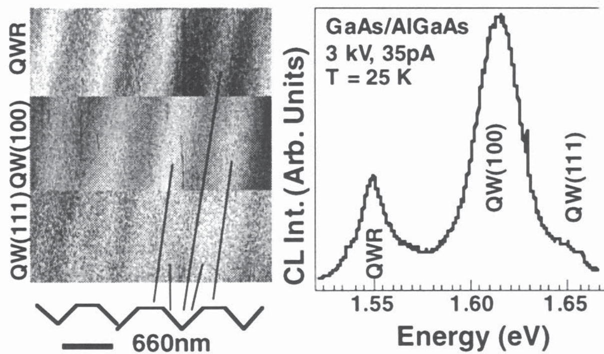

Figure 10. The spectrum from a single QWR structure exhibits three peaks. In this case, the single QWR structure was grown on a 660 nm period grating. In the top view images of the three peaks, their origin can be identified. Especially significant is the double periodicity of the side QW. Note the high spatial resolution of the image of the side QW.

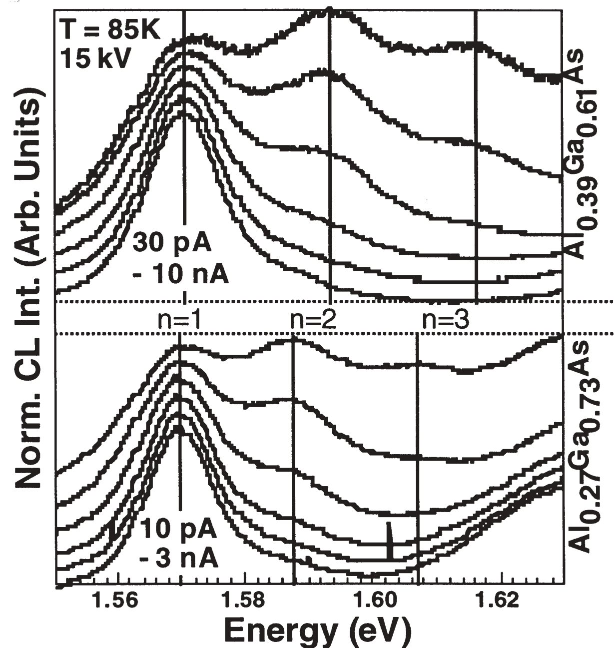

Figure 11. A series of normalized spectra from a QWR sample, recorded with increasing probe currents. The lowest probe current corresponds to the spectrum at the bottom and the ratio of the probe currents in consecutive spectra is 3.3. As the excitation density is increased, emission from excited subbands can be observed. This is shown for two different compositions of the barriers, where the spacing between the subbands increases with Al content.

on top will restore the original shape of the groove. Consequently, the shape of the QWR is determined by the growth conditions and can be reproduced from growth run to growth run as well as within a stack of QWRs.

Related to this variation in the shape of the growth front is the variation in the Ga incorporation in the AlGaAs barrier. The difference is most notable at the bottom of the groove, where a higher Ga content is found. This can be observed in the TEM image of Figure 7, as a dark stripe stretching along the stack of the QWRs. This stripe is well defined both in composition and in width. In fact, this forms a *vertical* QW (VQW). In contrast to the conventional QWs, that are intentionally grown with switching of the sources during growth, the VQWs form by self-ordering. The shape and depth of the VQWs are given only by the growth conditions. Thus, not just the thickness of the QWR crescent deviates from the thickness of the GaAs QW grown on a planar substrate, but also the alloy composition is modified due to the non-planar growth. The V-groove structure is generally defined by near-{111}A planes in the grooves, {311}A planes on the verges of the grooves and (100) planes outside the grooves. Depending on the growth conditions, the growth rate of the AlGaAs barrier of the three planes varies, which is mainly reflected in the extension of the {311}A planes. This determines the shape of the V groove. Equally important is the growth rate of the GaAs layer, which can lead to up to three (on the (100), {311}A and {111}A planes) significantly different QW thicknesses and the formation of the QWR at the bottom of the groove. This results in several emission peaks with well-defined spatial origin (Christen *et al.,* 1992; Grundmann *et al.,* 1995b; Gustafsson *et al.,* 1995a,b).

CL can be very important and useful for identifying the spatial origin of these different peaks. This has been shown in several publications (Christen *et al.,* 1992; Clausen *et al.,* 1990b; Grundmann *et al.,* 1995b; Gustafsson *et al.,* 1995a,b; Kapon *et al.,* 1992b). Figure 8 displays a series of images of a typical sample (a stack of 10 GaAs QWRs, grown on a V-groove grating with a period of 3.5 μm) in side view. The spatially averaged spectrum of the sample contains 3 peaks. When a series of images is made with the detection varied from the low to the high energy peak, the origins of the peaks can be identified. At 1.60 eV the emission originates from the QWRs at the bottom of the groove. At 1.66 eV the emission appears from the top of the ridges between the grooves: the top (100) QW. With the detection at 1.73 eV, the emission appears from the middle of the side walls: the side wall QW. An interesting feature can be observed as the detection wavelength is varied around the 1.73 eV of the side QW. The spatial origin of the emission moves upwards on the side walls when detecting a lower

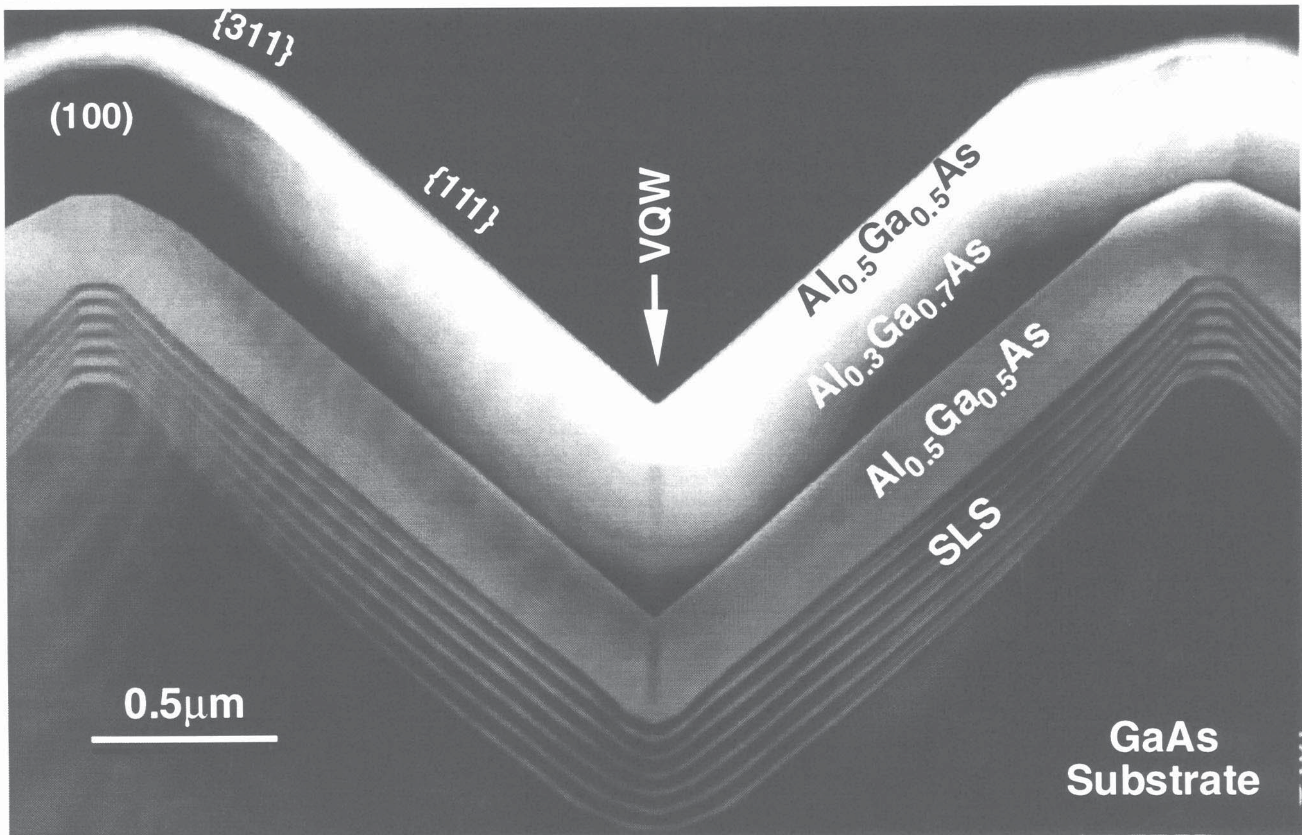

Figure 12. A DF TEM image of a full period of a typical VQW structure. From bottom to top: V-grooved GaAs substrate, superlattice, $Al_{0.50}Ga_{0.50}As$ lower barrier, $Al_{0.30}Ga_{0.70}As$ core layer and finally $Al_{0.50}Ga_{0.50}As$ upper barrier.

energy and moves downwards when detecting a higher energy. This reveals that there is a thickness gradient of the side wall QW. This gradient is also evident in the series of spectra of Figure 9, which shows a series of spectra in spot mode of a similar structure. The spot has been moved from one groove to the nearest groove. The trend of the gradual shift in energy position of the side wall peak is obvious.

The 3.5 μm period of the grating is very suitable for CL studies, but useful information can be obtained even from sub-micron period gratings (Gustafsson *et al.,* 1995a). These structures usually have the advantage of more intense signal from the QWR, mainly an effect of the higher filling factor (more QWRs per surface area). Figure 10 shows the CL spectrum and parts of three top view images of a similar structure as in Figures 8 and 9: here, however, the period of the grating is 0.66 μm and the structure consists of a single GaAs layer, i.e., a single QWR per groove. The spectrum of the structure shows three components: the QWR at lower energy, the top QW and the side QW. In the top view images of the structure, the distinction between the two QW parts can be made. The image covers one area, but it is made from parts of three different scans, obtained using the three emission peaks of the structure. The top part shows the QWR image from the first part of the area, the middle part is an image of the main QW peak from the middle of the area and the bottom is the image of the high energy QW peak from the bottom of the area. The contrast variations of the main peak are fully out of phase with the corresponding variations in the QWR image, whereas the high energy peak shows the double periodicity expected of the side wall QW emission. The identification of the low energy QW peak as the top QW and the high energy QW peak as the side QW is consistent with the case of the 3.5 μm-pitch grating. It is worth pointing out that the experimental resolution in the images is in some sense better than 300 nm (half the pitch of the grating).

As mentioned above, one of the important signatures of a QWR is the 1D subbands. There are several ways to demonstrate this property. One of the most reliable ways to observe these subbands, is to use a photoluminescence

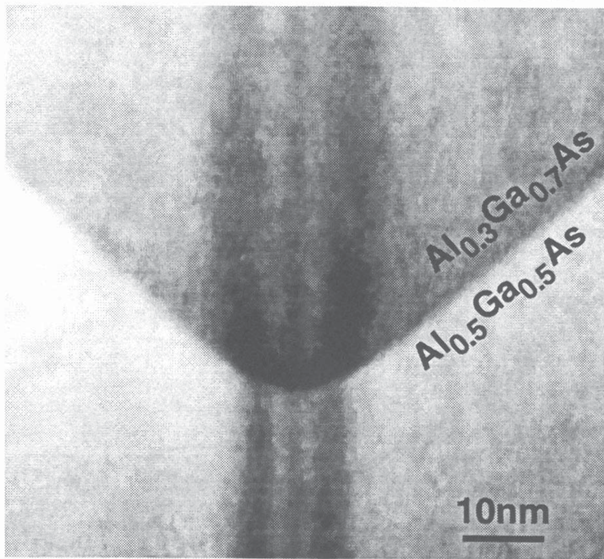

Figure 13. A DF TEM image of the central region of the VQW structure of Figure 12 containing 3 layers of different Al content. The typical triple branch structure of the VQW can be observed.

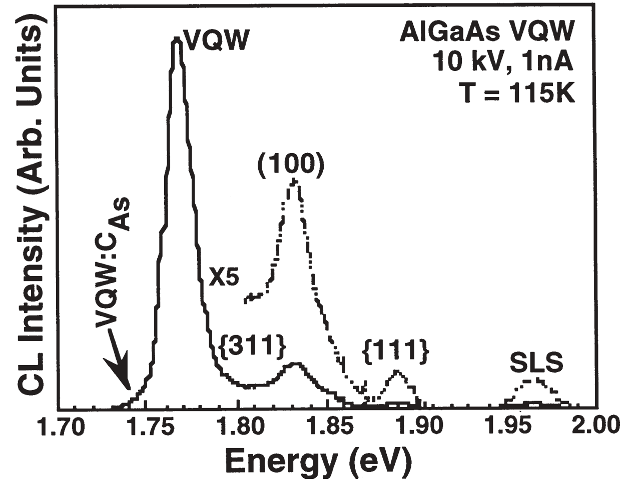

Figure 14. A typical spatially averaged spectrum of a sample with an $Al_{0.21}Ga_{0.79}As$ core region, where the peaks have been identified by CL imaging and spot mode spectra.

(PL) based technique known as PL excitation (PLE) spectroscopy. This technique will reveal the actual band structure of the QWR. Other ways to observe this structure is to use very high excitation densities, where the emission from the ground state is saturated and the emission from the exited states can be obtained. This can be done either by high intensity PL or by CL at high probe currents (Grundmann *et al.,* 1995b; Gustafsson *et al.,* 1995b; Samuelson *et al.,* 1994). The advantage of the CL measurements is the relatively small excitation volume, compared with PL. In Figure 11 we show spectra from two different samples, with different composition of the barrier. This leads to a larger subband separation in the sample with the higher Al content barrier. This can be observed in the figure as a larger spacing of the series of peaks (n=1, 2, 3) related to the QWR.

Vertical Quantum Wells

The VQW is interesting in itself from a phenomenological point of view. The formation of the VQW is an intrinsic property of the growth on non-planar substrates, as discussed above. Furthermore, it forms without any need of precise control of the thickness of the normal lateral QWs. It is even possible to make QW devices, particularly lasers, based on these self-organized VQWs (Kapon *et al.,* 1995b). In order to make these types of laser devices, it is essential

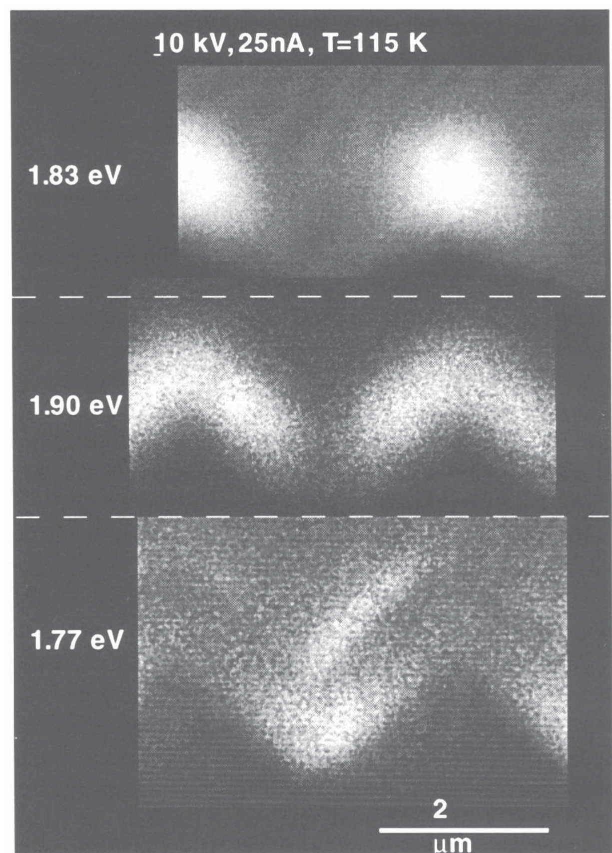

Figure 15. The origin of the major peaks from the VQW structure of Figure 14 can be revealed by monochromatic imaging.

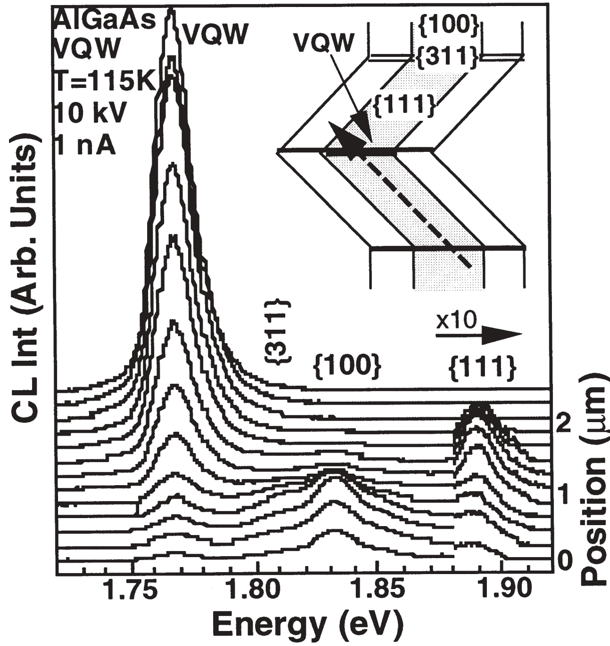

Figure 16. A series of spot-mode spectra, recorded along the {111} side wall, from the ridge to the bottom (bottom to top in the figure). The identification of the peaks in Figure 15 can be confirmed and the 1.89 eV peak can be identified to originate in the {111} region.

---

to understand the spatial origin of the emission peaks from the structure itself. Figure 12 shows a DF TEM image of one 3.5μm period of a typical VQW sample consisting of an $Al_{0.50}Ga_{0.50}As$-GaAs superlattice, an $Al_{0.50}Ga_{0.50}As$ lower barrier, an $Al_{0.30}Ga_{0.70}As$ core layer and an $Al_{0.50}Ga_{0.50}As$ upper barrier. The VQW in the V-groove can be observed as a dark stripe. It is also worth noting the contrast on top of the ridges. This area appears to contain narrow regions of both increased and decreased Ga content. Figure 13 shows the VQW at higher magnification, where the VQW in both the $Al_{0.30}Ga_{0.70}As$ core layer and $Al_{0.50}Ga_{0.50}As$ lower barrier can be seen. The VQWs both have a distinct triple branch structure, which is a signature of low-pressure MOCVD (Biasiol *et al.,* 1996; Gustafsson *et al.,* 1995b). It can be observed that the width of the VQW increases with increasing Ga content in the barrier.

The spatially averaged CL spectra of the structure, presented in Figure 14, contains several peaks. There is one dominant feature and several other minor peaks. Side view monochromatic images of three of the peaks are shown in Figure 15. From this it can be concluded that the 1.77 eV peak is the peak of the VQW and the spatial origin of the 1.83 eV peak can be attributed to the ridges of the structures. TEM images of the structure identify a high Ga content area related to the {311} region. However, the spatial origin of the 1.89 eV emission is not as clear, except that the region around the VQW can be excluded. The major peaks are the only peaks that are intense enough to allow conclusions to be drawn regarding their spatial origin. To reveal the origin of the minor peaks it is necessary to make a series of spot mode spectra along several lines. Figure 16 shows one of these scans, along the side wall of the structure.

Here the identification of the two major peaks is confirmed and the origin of the minor peaks can be identified. This especially applies to the emission peak from the barrier on the {111} side walls. Making similar line scans across the structure at 5 K, 77 K and 115 K it is possible to identify the emission from the superlattice as well. An interesting feature is a low intensity peak that appears as a shoulder on the low energy side of the VQW peak in the spatially averaged spectrum. It has the same spatial origin as the VQW peak. The intensity ratio of the VQW peak to the shoulder peak varies from groove to groove, which leads us to associate these peaks with impurities in the structures.

Impurities in Low-Dimensional Structures

The concept of impurities in semiconductors is usually treated as an omnipresent property of the material. However as the size of the structures gets smaller, this is not always necessarily true. In a QW, the energy position of an acceptor level depends critically on the position. An acceptor in the middle of the QW can have a 4 times larger binding energy than an acceptor near the barrier-to-QW interface (Masselink *et al.,* 1986). Not only the position in the QW plays a role, but as the thickness of the QW is reduced, the spacing between the impurities can be on the same scale as, or larger than, the carrier diffusion length. This means that the properties of certain areas of the QW can be influenced by the impurities, whereas other parts are intrinsic. This effect becomes more prominent in QWRs and quantum dots (QDs). Consider a QWR with a 5×100 nm^2 cross-section and a relatively low impurity concentration of $1*10^{16}$ cm^{-3}, or in a more relevant unit 10 $\mu m^{-2} nm^{-1}$. In this case, there is, on average, one impurity per 0.2 μm of QWR length. For the QD the situation is even more acute. A QD of 5×100×100 nm^3 will on average contain 0.5 impurity, i.e. every second QD will contain an impurity. This has the consequence that half the QDs will have different energy levels even though they have identical sizes!

It is of fundamental interest, as well as of applications interest, to study the behavior of impurities in low-dimensional semiconductors. Here we will demonstrate how single impurities can be isolated and studied by CL (Samuelson and Gustafsson, 1995). The example considered is the carbon acceptor in a 5 nm thick GaAs QW in between AlGaAs barriers. Carbon is chosen as it is the background

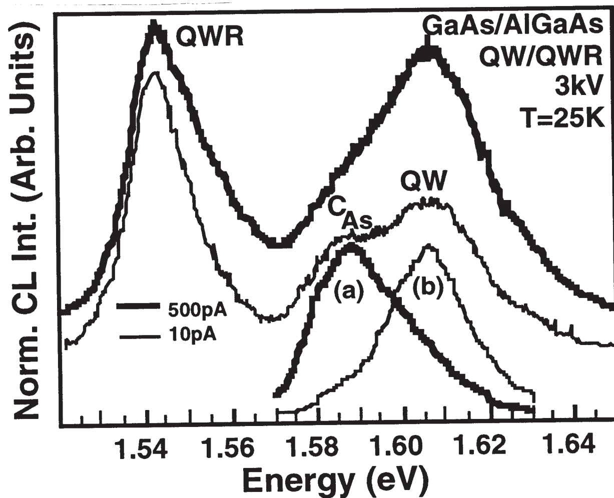

Figure 17. At a normal CL probe current of 500 pA, the spectrum of a V-groove QWR structure exhibits two peaks: one from the QWR and one from the QW. By reducing the probe current to 10 pA, a feature appears on the low-energy side of the QW peak, which is identified as the emission via carbon acceptors in the QW. In the spot mode spectra, the two features can be isolated: (**a**) a spectrum with almost only C_{As} emission and (**b**) only intrinsic QW emission.

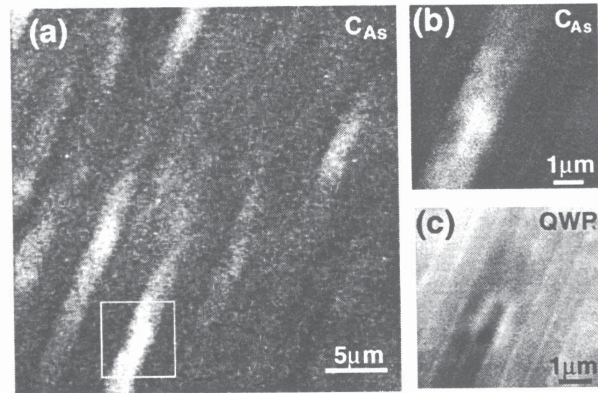

Figure 18. Single impurities can also be found in the QWR of the sample of Figure 17 by detecting the emission at an energy, 25 meV below the QWR peak. (**a**) the bright spots corresponding to the single C_{As} in the QWR are separated several tens of μm along the QWR. (**b**) and (**c**) show a higher magnification of the area outlined in white in (a). (**b**) is the image of the C_{As} emission, a single C_{As} can be observed. (**c**) shows the same area, but detecting the intrinsic QWR emission, where the individual QWRs can be observed.

impurity in MOCVD grown GaAs, typically $1*10^{15}$ cm^{-3}. The binding energy for the C_{As} is about 35 meV (Masselink *et al.,* 1986), whereas the exciton binding energy is approximately 10 meV (Herman *et al.,* 1991). In the 5 nm GaAs QW in between $Al_{0.35}Ga_{0.65}As$ barriers, a thickness variation of 1 ML introduces a difference in the confinement energy of ~5 meV, which makes the distinction between the spectral signature of a thickness variation and an impurity clear. The $1*10^{15}$ cm^{-3} density corresponds to an in-plane inter-impurity distance (D_{imp}) ~0.5 μm on average. In thin stripes of QW material it is possible to increase D_{imp}, but still keep the signature of the QW. A very efficient way to fabricate these stripes is to use the technique of QWR fabrication by growth on V-grooved substrates, but to study the QW on the planar region in between the grooves, rather than the QWRs. These stripes are isolated by the thinner QWs (higher energy) on the side walls of the groove. The higher energy of the side QW provides an effective barrier for diffusion between the different stripes. The fact that the side QWs are thinner means that their spectral features will appear on the high-energy side of the planar QW peak, whereas the C_{As} peak appears on the low-energy side. The V-groove approach has advantages over the more obvious way, i.e. etching out the stripes in an existing QW, which tends to result in non-radiative recombination on the surface of the side walls as well as damaged layers (optically inactive "dead layers") on the sides.

Figure 17 shows spectra of a V-groove QWR sample. At extremely low excitation densities, e.g. 10 pA and 5 kV, there are three spectral features. The QWR at 1.54 eV, the planar QW at 1.61 eV and at 1.59 eV a peak attributed to recombination via C_{As} in the QW. As expected, this peak saturates very easily and can hardly be distinguished with a probe current of 500 pA. In top view images of the two QW related peaks show complimentary behaviour. It is also possible to isolate the two emission peaks in spot mode spectra. This is also illustrated in Figure 17. This possibility to isolate the two spectral components further supports the interpretation of the peaks. Further evidence can be obtained by counting the number of bright spots and to relate that to the corresponding density. This corresponds well to the expected density of ~$1*10^{15}$ cm^{-3}.

The signature of single C_{As} can also be observed in the QWR itself. With the much smaller cross section of the QWR, the spacing between the impurities is expected to be much larger. Figure 18 shows the image of the QWR peak, which exhibits the bright lines, corresponding to the QWRs. This image also shows the same area, but with the detection set to a 25 meV lower energy. In this latter image, one bright spot can be observed. The interesting point is that this image illustrates the efficiency of excitation transfer into a

single segment of the QWR. For several μm along the QWR, the area between two adjacent QWRs supplies carriers to the segment containing the impurity.

Summary

We have demonstrated the applications of cathodoluminescence to several low-dimensional semiconductor structures. High-quality quantum wells exhibit emission peaks that originate in areas of different thicknesses. These differ by a single monolayer. We have demonstrated that though it is possible to make images, showing complimentary behaviour of the peaks involved, care has to be taken not to over-interpret the images in terms of extended monolayer-flat islands. In the case of complicated quantum wire and vertical quantum well structures, we have first shown that cathodoluminescence can be useful for determining the spatial origin of the various emission peaks. Then we have demonstrated how the subband structure of the quantum wire can be studied, by varying the excitation density. Finally, we have shown how single impurities can be located in both quantum wells and quantum wires.

Acknowledgments

The large number of samples used in this study were provided by several sources: W. Seifert at Lund University; G. Vermeire and P. Demeester at IMEC-Gent; F. Reinhardt, G. Biasiol, A. Rudra and J.-F. Carlin at IMO-Ecole Polytechnique Fédérale Lausanne (EPFL); and C. Caneau at Bellcore. A number of people have contributed to this article via fruitful discussions: L. Samuelson at Lund University; S. Nilsson at IHP-Frankfurt-Oder and D. Oberli, F. Vouilloz and E. Marinet at IMO-EPFL. Various parts of this work have been supported by the Technical Science Research Council (TFR), The Natural Science Research Council (NFR) and the National Board for Industrial and Technical Development (NUTEK) in Sweden and by Fonds National Suisse de la Recherche Scientifique in Switzerland. Part of the electron microscopy work was performed at Centre Interdépartemental de Microscopie Electronique at EPFL.

References

Araújo D, Pacheco F, Carlin J-F, Rudra A, Molina SI, García R (1994) Cathodoluminescence and transmission electron microscopy study of island formation on InAs/InP QW structures during growth interruptions. In: Defect Recognition and Image Processing in Semiconductors and Devices. Jiménez J (ed.) Institute of Physics Publishing, Bristol. pp. 335-338.

Biasiol G, Reinhardt F, Gustafsson A, Martinet E, Kapon E (1996) Structure and formation of AlGaAs V-groove vertical quantum wells grown by low pressure organometallic chemical vapor deposition. Appl. Phys. Lett. **69**, 2710-2712.

Bimberg D, Christen J, Fukunaga T, Nakashima H, Mars DE, Miller JN (1987) Cathodoluminescence atomic scale images of monolayer islands at GaAs/GaAlAs interfaces. J. Vac. Sci. Technol. B **5**, 1191-1197.

Carlin J-F, Rudra A, Houdré R, Ruterana P, Ilegems M (1992) Effect of growth interruptions on ultra-thin InAs/InP quantum wells grown by chemical beam epitaxy. J. Crystal Growth **120**, 155-156.

Christen J, Grundmann M, Bimberg D (1991) Scanning cathodoluminescence microscopy: A unique approach to atomic-scale characterization of hetero-interfaces and imaging of semiconductor inhomogenieties. J. Vac. Sci. Technol. B **9**, 2358-2368.

Christen J, Kapon E, Colas E, Hwang DM, Schiavone LM, Grundmann M, Bimberg D (1992) Cathodoluminescence investigations of lateral carrier confinement in GaAs/AlGaAs quantum wires grown by OMCVD on non-planar substrates. Surf. Sci. **267**, 257-262.

Clausen EM Jr, Harbison JP, Florez LT, Van der Gaag B (1990a) Assessing thermal Cl_2 etching regrowth as methods for surface passivation. J. Vac. Sci. Technol. B **8**, 1960-1965.

Clausen EM Jr, Kapon E, Tamargo MC, Hwang DM (1990b) Cathodoluminescence imaging of patterned quantum well heterostructures grown on nonplanar substrates by molecular beam epitaxy. Appl. Phys. Lett. **56**, 776-778.

Dingle R (1975) Confined carrier quantum states in ultrathin semiconductor heterostructures. In: Festkörperprobleme XV, Advances in Solid State Physics. Queisser HJ (ed.) Vieweg, Braunschweig pp. 21-48.

Forchel A, Leier H, Maile BE, Germann R (1988) Fabrication and optical spectroscopy of ultra small III-V semiconductor structures. In: Festkörperprobleme 28, Advances in Solid State Physics. Rössler U (ed.) Vieweg, Braunschweig pp. 99-119.

Grundmann M, Christen J, Joschko M, Stier O, Bimberg D, Kapon E (1994) Recombination kinetics, intersubband relaxation in semiconductor quantum wires. Semicond. Sci. Technol. **9**, 1939-1945.

Grundmann M, Christen J, Ledentsov NN, Böhrer J, Bimberg D, Ruvimov SS, Werner P, Richter U, Gösele U, Heydenreich J, Ustinov VM, Egorov AYu, Zhukov AE, Kop'ev PS, Alferov ZhI (1995a) Ultranarrow luminescence lines from single quantum dots. Phys. Rev. Lett. **74**, 4043-4046.

Grundmann M, Christen J, Bimberg D, Kapon E (1995b) Electronic and optical properties of quasi-one-dimensional carriers in quantum wires. J. Nonlinear Opt. Mater. **16**, 99-140.

Gustafsson, Samuelson L (1994) Cathodo-luminescence imaging of quantum wells: The influence of exciton transfer of the apparent island size. Phys. Rev. B **50**, 11827-11832.

Gustafsson A, Samuelson L, Hessman D, Malm J-O, Vermeire G, Demeester P (1995a) Characterization of a single-layer quantum wire structure grown directly on a submicron grating. J. Vac. Sci. Technol. B **13**, 308-317.

Gustafsson A, Reinhardt F, Biasiol G, Kapon E (1995b) Low-pressure organometallic chemical vapor deposition of quantum wires on V-grooved substrates. Appl. Phys. Lett. **67**, 3673-3675.

Herman MA, Bimberg D, Christen J (1991) Hetero-interfaces in quantum wells and epitaxial growth processes: Evaluation by luminescence techniques. J. Appl. Phys. **70**, R1-52.

Kapon E (1992) Quantum wire lasers. Proc. IEEE **80**, 398-410.

Kapon E, Tamargo MC, Hwang DM (1987) Molecular beam epitaxy of GaAs/AlGaAs superlattice heterostructures on nonplanar substrates. Appl. Phys. Lett. **50**, 347-349.

Kapon E, Walther M, Christen J, Grundmann M, Caneau C, Hwang DM, Colas E, Bhat R, Song GH, Bimberg D (1992a) Quantum wire heterostructures for optoelectronic applications. Superlattices and Micro-structures **12**, 491-499.

Kapon E, Kash K, Clausen EM Jr, Hwang DM, Colas E (1992b) Luminescence characteristics of quantum wires grown by organometallic chemical vapor deposition on nonplanar substrates. Appl. Phys. Lett. **60**, 477-479.

Kapon E, Biasiol G, Hwang DM, Colas E (1995a) Seeded self-ordering of GaAs/AlGaAs quantum wires on non-planar substrates. Microelectronics J. **26**, 881-886.

Kapon E, Dwir B, Pier H, Gustafsson A, Bonard J-M, Hwang DM, Colas E (1995b) Lasing in self-ordered vertical quantum well heterostructures. Technical Digest Vol. **16** / Quantum Electronics and Laser Science Conference. pp. 235-236.

Leon R, Petroff PM, Leonard D, Fafard S (1995) Spatial resolved visible luminescence of self-assembled semiconductor quantum dots. Science **267**, 1966-1968.

Liu X, Nilsson S, Samuelson L, Seifert W, Souza PL (1993) Extended monolayer flat islands and exciton dynamics in $Ga_{0.47}In_{0.53}As$/InP quantum-well structures. Phys. Rev. B**47**, 2203-2215.

Masselink WT, Chang Y-C, Morkoç H, Reynolds DC, Litton CW, Bajaj KK, Yu PW (1986) Shallow impurity levels in AlGaAs/GaAs semiconductor quantum wells. Solid-State Electronics **29**, 205-213.

Merz JM, Petroff PM (1991) Making quantum wires and boxes for optoelectronic devices. Mater. Sci. Eng. B**9**, 275-284.

Nilsson S, Gustafsson A, Samuelson L (1990) Cathodoluminescence observation of extended monolayer-flat terraces at the heterointerface of GaInAs/InP single quantum wells grown by metalorganic vapor phase epitaxy. Appl. Phys. Lett. **57**, 878-890.

Petroff PM, Cibert J, Gossard AC, Dolan GJ, Tu CW (1987) Interface structure and optical properties of quantum wells and quantum boxes. J. Vac. Sci. Technol. B **5**, 1204-1208.

Samuelson L, Gustafsson A (1995) Imaging and spectroscopy studies of individual impurities in quantum structures. Phys. Rev. Lett. **74**, 2395-2398.

Samuelson L, Gustafsson A, Lindahl J, Montelius L, Pistol M-E, Malm J-O, Vermeire G, Demeester P (1994) Scanning tunneling microscope and electron beam induced luminescence in quantum wires. J. Vac. Sci. Technol. B **5**, 2521-2526.

Seifert W, Fornell J-O, Ledebo L, Pistol M-E, Samuelson L (1990) Single mono-layer quantum wells of GaInAs/InP grown by metalorganic vapor phase epitaxy. Appl. Phys. Lett. **56**, 1128-1130.

Tiwari S (1994) Operaton of strained multi-quantum wire lasers. Low dimensional structures prepared by epitaxial growth or regrowth on patterned substrates. Ebel K, Petroff PM, Demeester P (eds). Kluwer Academic Publishers, Dordrecht 335-344.

Tiwari S, Pettit GD, Milkove, KR, Legouse F, Davis RJ, Woodall JM (1994) High efficiency and low threshold current strained V-groove quantum-wire lasers. Appl. Phys. Lett. **64**, 3536-3538.

Warwick CA, Jan WY, Ourmazd A (1990) Does luminescence show semiconductor interfaces to be atomically smooth? Appl. Phys. Lett. **56**, 2666-2668.

Yacobi BG, Holt DB (1990) Cathodoluminescence Microscopy of Inorganic Solids. Plenum Press, London. pp. 55-88.

Discussion with Reviewers

C. E. Norman: It is true that at 5 kV, the resolution will be limited by the electron range (approximately 140 nm in InP) plus diffusion. Would not an acceleration voltage of 1 or 2 kV offer a better chance of resolving individual islands.

Authors: A lower acceleration voltage could offer a higher resolution under certain conditions. In this sample, the InP layer covering the islands is about 100 nm. This means that the main excitation would be above the islands, using a lower acceleration voltage, The resulting resolution might even be worse. Another factor to consider is that the spot size of many (older) SEMs increases with reduced acceleration voltage for a given probe current, which may even *reduce* the resolution.

C. E. Norman: There is currently a great deal of interest in

the growth of self-organized QDs in lattice mismatched systems, along similar lines to the island formation demonstrated in Figures 5 and 6 for InAs/InP. Can the authors envisage suitable imaging conditions and specimen geometry which will enable *individual* QDs to be *spatially* resolved using CL.

Authors: There are several reports claiming to resolve individual QDs grown by this technique (Carlsson *et al.,* 1994; Grundmann *et al.,* 1995a; Leon *et al.,* 1995) The simplest way to ensure that you are looking a single QDs is to have a low enough density <10^{-8} cm^{-2}, where the QDs are separated by >1 μm. Then there sould be no doubt of the identification (Carlsson *et al.,* 1994). Increasing the density, it is still possible to identify the individual QDs. This can be achieved, by using thin TEM samples in an STEM, where it is possible to compare the CL images with the TEM images, thus enabling a direct correlation between QDs and emission (Leon *et al.,* 1995). Here it is possible to observe single QDs with a spatial resolution of ~500 nm, even if their emission is identical. However, since a normal density of QDs is ~10^{-10}-10^{-11} cm^{-2}, with an average spacing of 35-100 nm, neither of these techniques would be sufficient. One approach would be to etch out small mesas, using a thin cap layer to minimize etch damages and e. g. aerosol particles as a mask, where a 50 nm diameter is achievable (Maximov *et al.,* 1993) . With a low density of particles <10^{-8} cm^{-2} it should be possible to do CL spectroscopy on individual QDs. The number of these mesas would still be high enough to get some statistics on the distribution of QDs.

G. Salviati: Independently on MOCVD and CBE growth conditions (with or without growth interruption procedures), there is evidence from the literature (see for instance Rigo *et al.* (1994), Salviati *et al.* (1993), and Streubel *et al.* (1992)) that As (max. incorporation about 30%) and P (max. incorporation about 15%) incorporation (neglecting As carry over (about 3%)) results in InAsP and GaInAsP extra layers at the InP/GaInAs/InP interfaces. The minimum thickness, calculated by high resolution TEM and high resolution X-ray diffraction investigations, is about 3-4 ML. Further, taking into account a possible compositional inhomogeneity in the extra layers on the growth plane and the associated strain, a CL peak shift of about 70-80 meV at 4 K can be induced. As a consequence, it seems hazardous to interpret the two micrographs of Figure 3 as direct maps of 4 and 5 ML thick areas, unless the compositional homogeneity, As and P incorporation and induced strain have been previously checked and possibly calculated.

Authors: All the samples in this series contain several QWs of different nominal thickness, ranging from 0.5 to 20 ML, plus a 50 nm thick reference layer. The samples were grown without rotation, resulting in a thickness gradient along the gas-flow direction in the reactor. We were able to observe a thickness gradient of the QWs as a shift in the peak position and a slight compositional gradient as a peak shift in the reference layer. For all but the thinnest QWs, the emission behaves the same, with a split into two peaks. In a series of spectra recorded along the thickness gradient, each individual peak stays in the same position, but the ratio between the peaks originating in the same QW is gradually changing (Liu *et al.,* 1993). As the peak on the low-energy side disappears, a peak appears on the high energy side. For the same distance, a thicker QW exhibits more of these discrete peaks than a thinner, consistent with the thickness gradient. The splitting of the peaks is larger in the thinner QWs, also consistent with thickness. Furthermore, using the model of interface layers (Streubel *et al.,* 1992) , we have been able to fit the energy position of the peaks in the samples. As mentioned in the text, the peak denoted 1 ML is the result of the exchange processes at the interfaces, and the other thicknesses, n ML, are n-1 ML of GaInAs plus the interface layers.

Clearly, a compositional variation would introduce an additional broadening of the peaks, but to the best of our knowledge, most compositional variations in (100) planar GaInAs layers are on a much smaller scale, <100 nm, than the intensity variations on the images of Figure 3. Another cause for peak position variations could be ordering, which could appear on this scale. However, the present layers are not grown under conditions where ordering of GaInAs can be expected. In short, with the full picture of the behaviour of emission from the QWs, we believe that the main cause for the splitting of the peaks from single QWs is a thickness effect, that can be modulated by a smaller effect of compositional variations.

It is worth pointing out that though we interpret the two emission peaks as originating in areas of different thickness, we do not interpret the images in Figure 3 as a direct map of the areas of different thicknesses. The figure is more likely be a map of variations in the density of much smaller islands (Gustafsson and Samuelson, 1994).

Additional References

Carlsson N, Seifert W, Petersson A, Castrillo P, Pistol M-E, Samuelson L (1994) Study of the two-dimensional—three-dimensional growth mode transition in metalorganic vapor phase epitaxy of GaInP/InP quantum-sized structures. Appl. Phys. Lett. **65**, 3093-3095.

Maximov I, Gustafsson A, Hansson H-C, Samuelson L, Seifert W, Wiedensohler A (1993) Fabrication of quantum dot structures using aerosol deposition and plasma etching techniques. J. Vac. Sci. Technol. A **11**, 748-53.

Rigo C, Campi D, Neitzert H C, Soldani D, Lazzarini L, Salviati G (1994) Optimization of growth-parameters of short-period InGaAs/InP superlattices for Wannier-Stark

modulators. Mater. Sci. Eng. B **28**, 305-309.

Salviati G, Ferrari C, Lazzarini L, Genova F, Rigo C, Schiavini G M, Taiarol F (1993) High resolution TEM and XRD study of interface composition inhomogeneities in CBE and MOCVD grown in (GaAs)P/InP multiple quantum wells. In: Microscopy of Semiconducting Materials. Cullis AG, Staton-Bevan AE, Hutchison JL (eds.). Institute of Physics Publishing, Bristol. pp. 471-476.

Streubel K, Härle V, Scholz F, Bode M, Grundmann M (1992) Interfacial properties of very thin GaInAs/InP quantum well structures grown by metalorganic vapor phase epitaxy. J. Appl. Phys. **71**, 3300-3306.